Nonlinear Optics (WiSe 2017/18)

Lecture 20: January 09, 2018

11 Terahertz generation and applications

11.1 Auston switch

11.2 Optical rectification

11.2.1 Optical rectification with tilted-pulse-fronts

11.2.2 Optical rectification by Quasi-Phase Matching (QPM)

11 Terahertz generation and applications

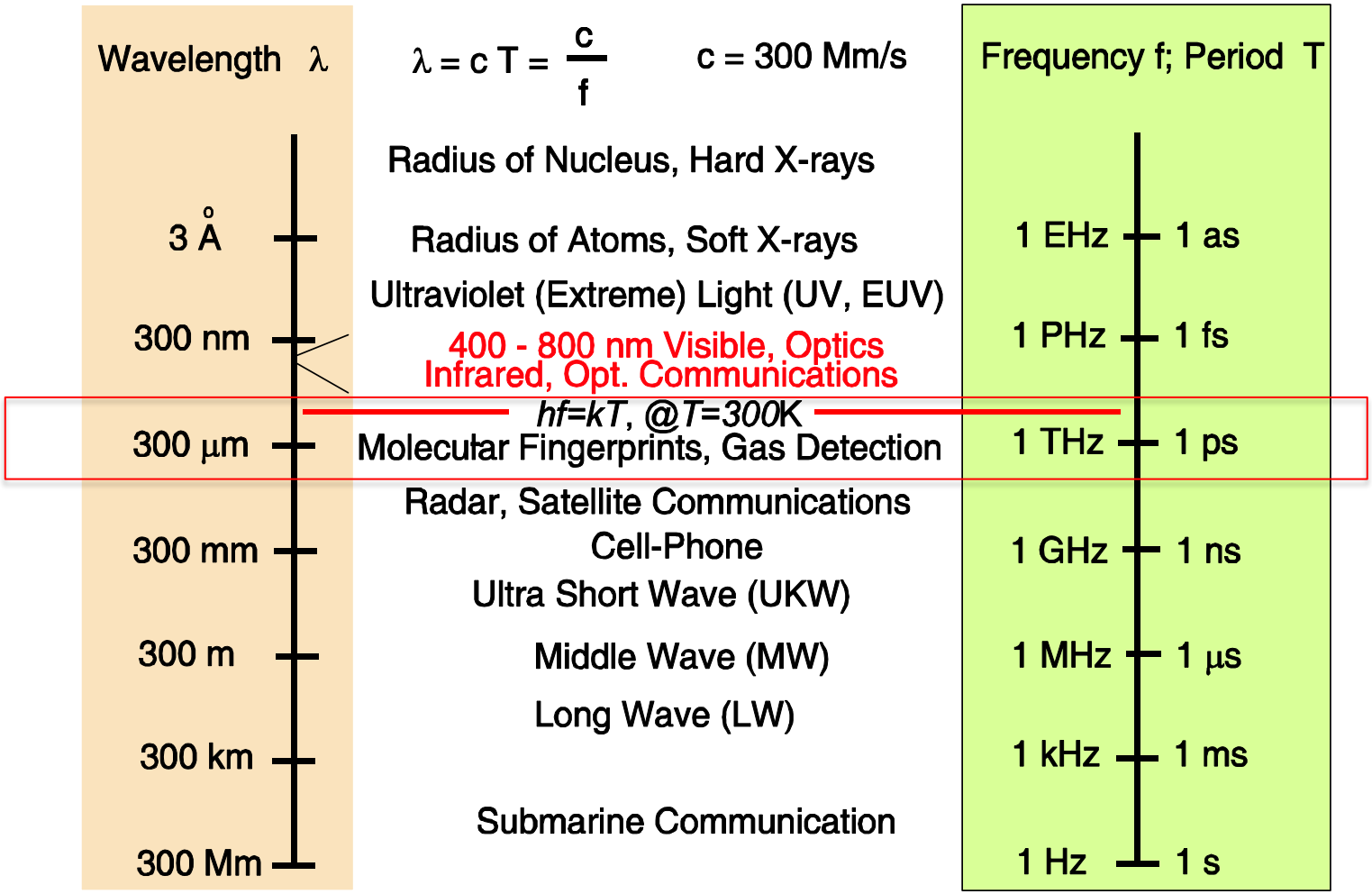

0.3 – 30 THz

THz Time Domain Spectroscopy

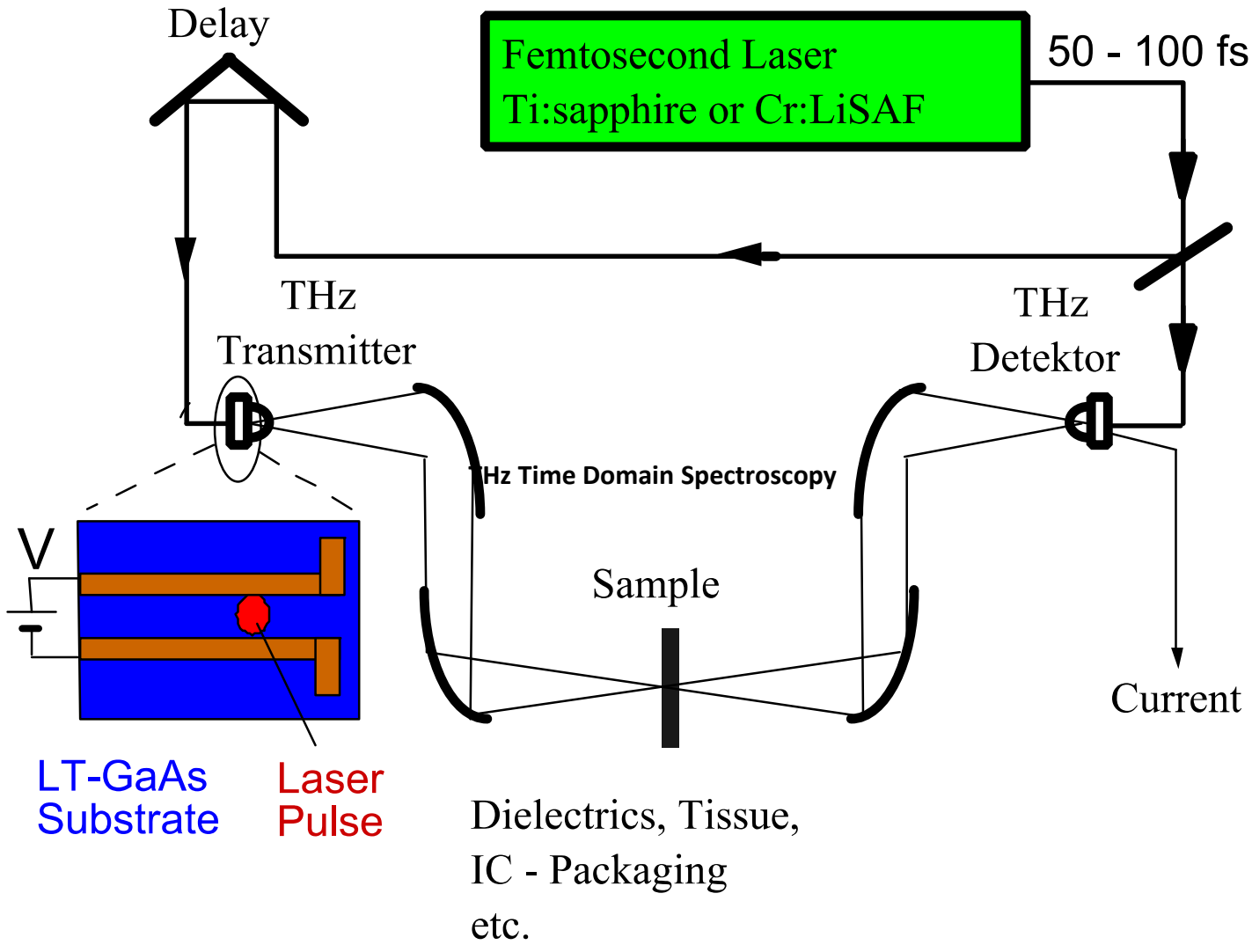

Fig. 11.1: THz pulses generated (a) and received (b) with photoconductive switches.

THz Time Domain Spectroscopy using optical rectification in GaAs

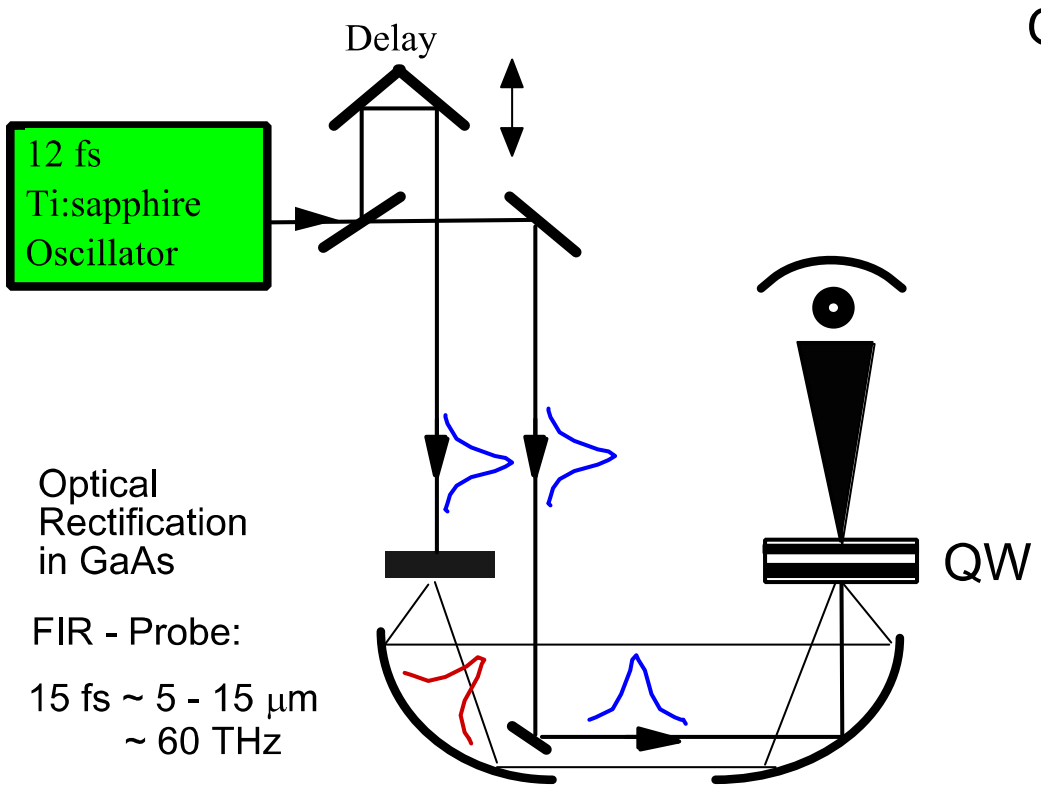

GaInAs/GaAs/AlAs

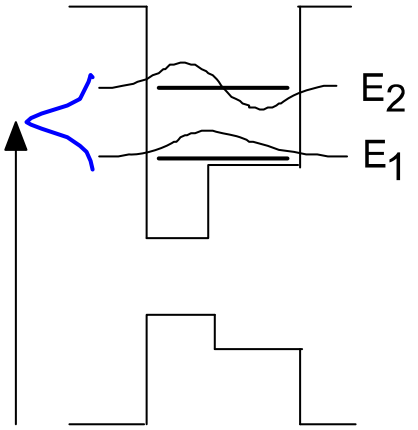

Optical Rectification in GaAs

FIR - Probe:

15 fs ~ 5 - 15 μm
~ 60 THz

6 fs > 100 THz

THz - OPOs
- OPAs

Quantum-Cascade Laser

Time Domain THz Spectroscopy

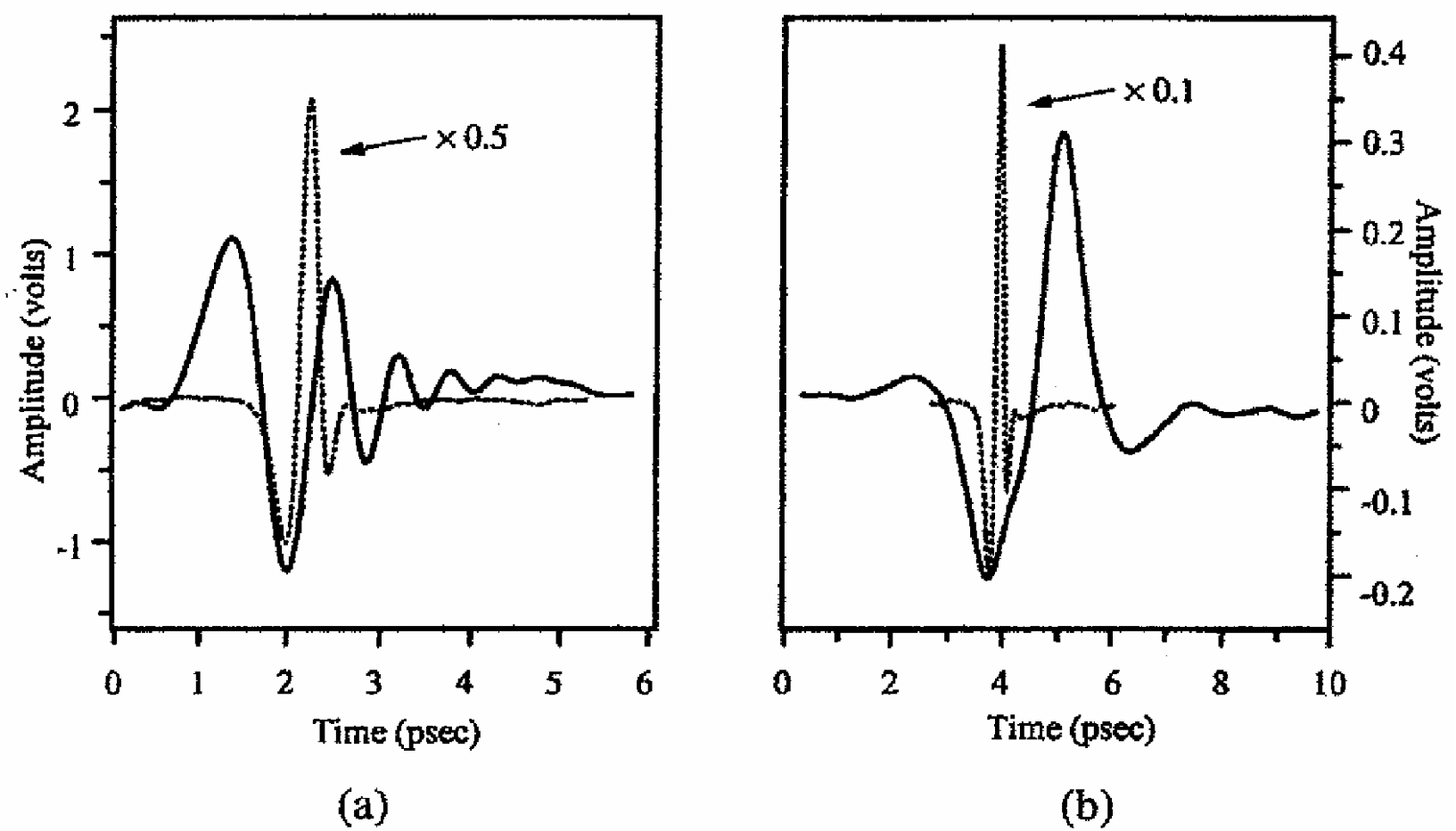

Figure 11.2: Terahertz waveforms modified by passage through (a) a 10 mm block of stycast and (b) a chinese fortune cookie. The dashed lines show the shape of the input waveform multiplied by 0.5 in (a) and by 0.1 in (b). In (a) the transmitted pulse exhibits a strong ”chirp” due to a frequency-dependent index, while in (b), pulse broadening indicates preferential absorption of high frequencies. [7]

Attosecond diffraction and spectroscopy of biomolecules

Damage-free structure

Undisturbed electronic structure

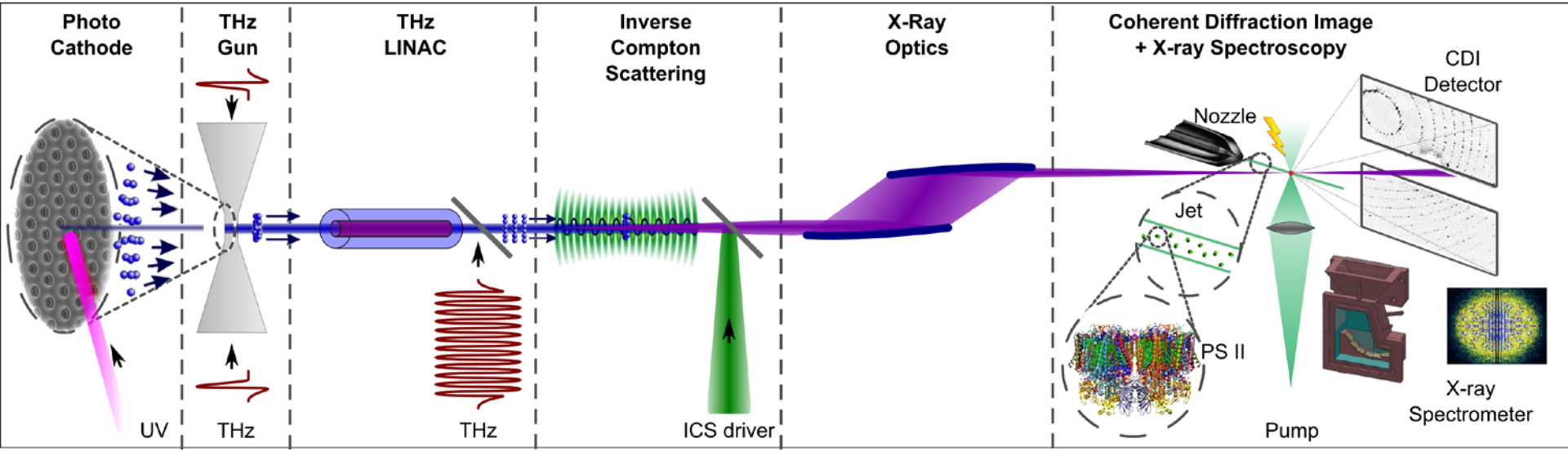

All laser driven, intrinsic attosecond synchronization

Only pico-second lasers at 1J-level necessary -> kHz operation

→ All optical driven fully coherent attosecond X-ray source:

- **→ has its own science case**
- **→ seeding of large scale FELs**
- **→ resolve access problem to large facilities**

THz Acceleration

Dielectrically Loaded Circular Waveguide

- Traveling wave structure is best for coupling broad-band single cycle pulses
- Phase-velocity matched to electron velocity with thickness of dielectric

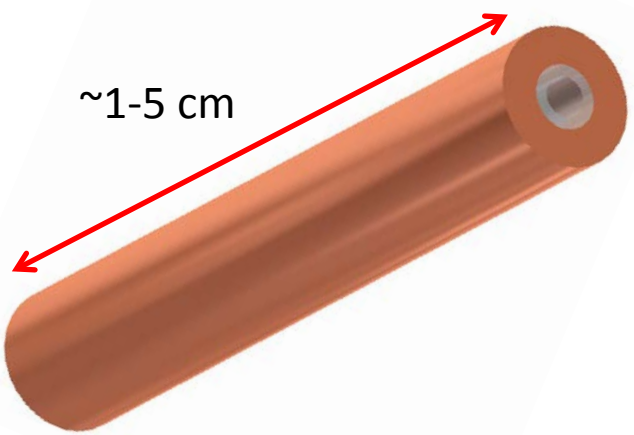

Copper Inner Diameter = 940 µm

Fused Silica Inner Diameter = 400 µm

Dispersion Relation

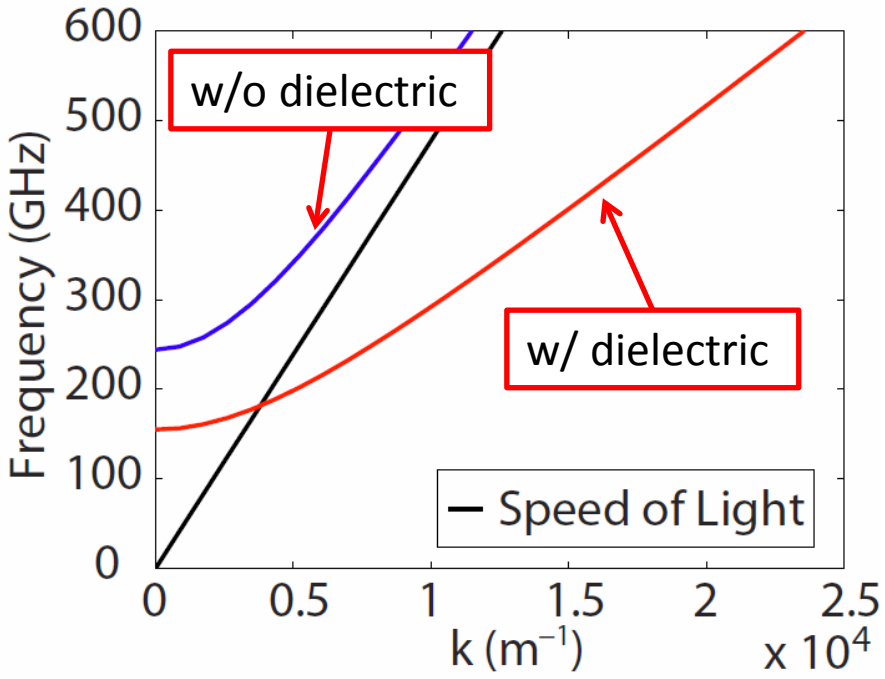

L.J. Wong et al., Opt. Exp. 21, 9792 (2013).

Terahertz-driven Linear Electron Acceleration

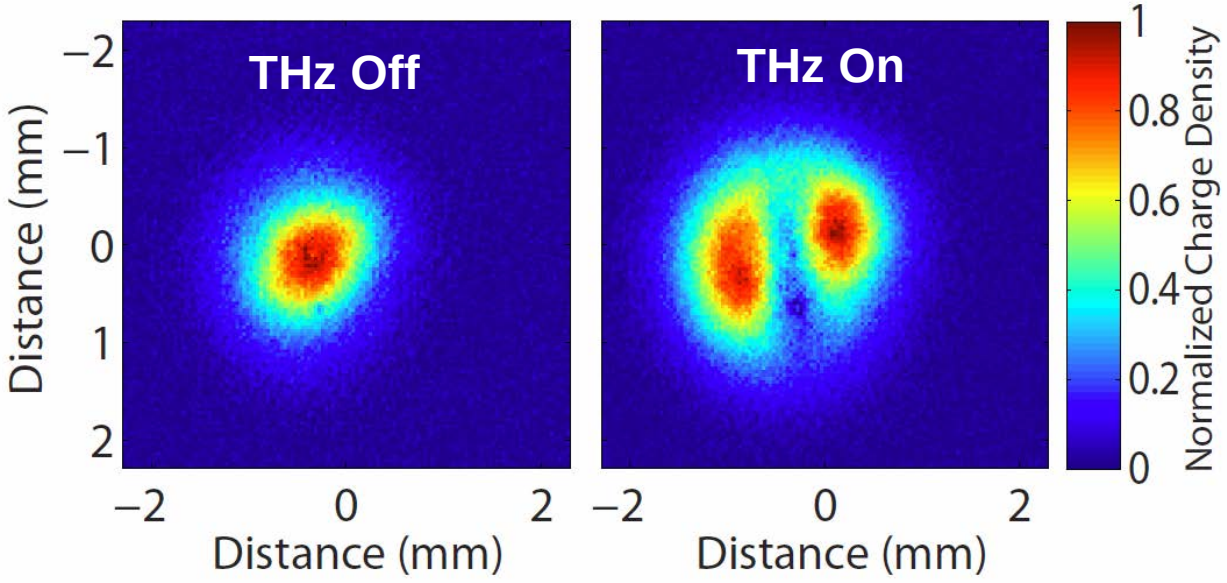

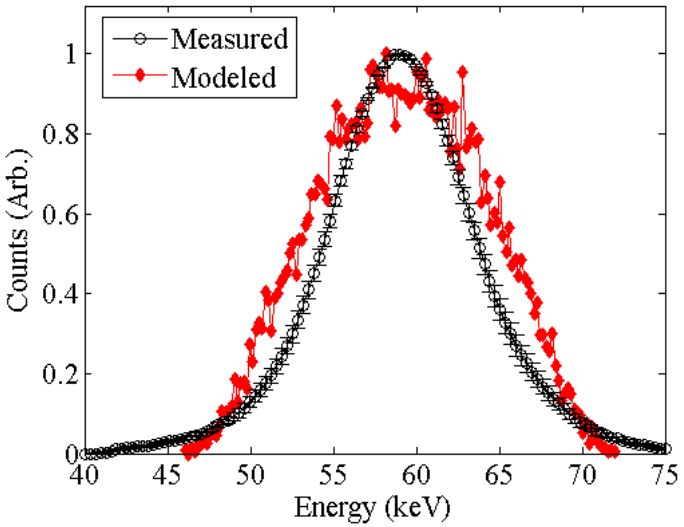

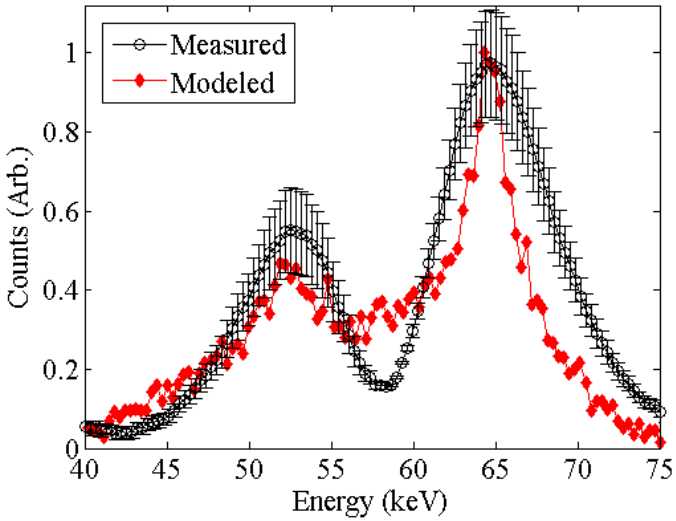

11.2 Optical rectification

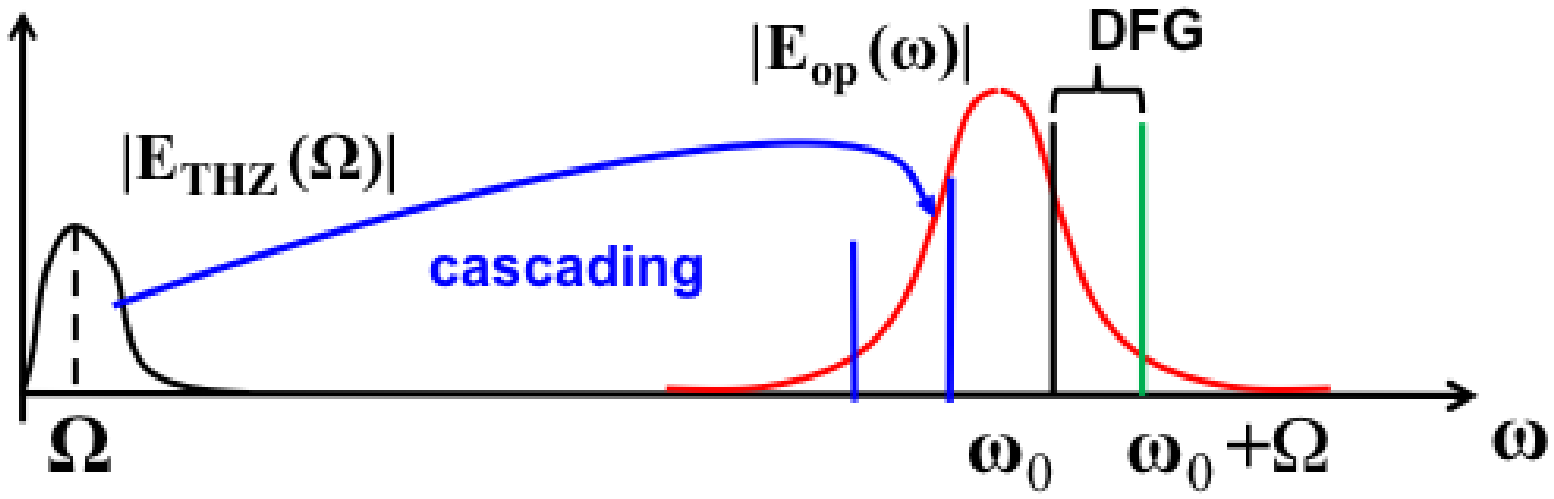

Figure 11.3: THz generation by DFG from two cw lines or from intrapulse spectral components. Once intense enough THz has been generated it acts back on the generating lines and creates additional down-shifted lines, which themselves again generate THz by DFG. This cascaded DFG process leads to a continuous down- shifting of the center of the optical spectrum.

THz Materialproperties I

crystal	ZnTe	$LiNbO_3$	$LiTaO_3$	GaP
opt. wl (μm)	0.8	1.06	1.06	1.06
opt. ref. index	2.85	2.16	2.14	3.11
THz ref. index	3.2	5.2	6.5	3.21
$\Delta n = n_{THz} - n_{g,opt}$	0.35	3.0	4.32	0.1
THz abs. (cm^{-1})	9.9	21.7	95	3.3
transp. range (μm)	0.55-30	0.4-5.2	0.4-5.5	0.55-10
band gap (eV)	2.26	3.7	5.65	2.25
nonlin. coeff. (pm/V)	d_{14}=23.1	d_{33}=152.4	d_{33}=145.2	d_{14}=21.7
nonlin. ref. index n_2 $\frac{10^{-15}cm^2/W}{\text{at } \lambda\ (\mu m)}$	120 at 1.06 71 at 0.8	0.91 at 1.06	0.37 at 1.06	20 at 0.78
FOM_1, long pulses	0.03	1	0.21	0.06
FOM_2, ultrashort pl.	0.74	1	0.64	1,67
FOM_3, Kerr-limited	0.00045	1	0.416	0.005

Table 11.1: Linear and nonlinear properties, and figures of merit (normalized to $LiNbO_3$) of crystals transparent in the 0-4 THz range and most widely used for optical THz generation according to Ref. [10].

THz Materialproperties II

crystal	GaSe	GaAs	ZGP	$CdSiP_2$
opt. wl (μm)	1.06	2.1	2.1	2.0
opt. ref. index	2.8	3.33	3.15	3.0
THz ref. index	3.26	3.6	3.37	3.05
$\Delta n = n_{THz} - n_{g,opt}$	0.34	0.18	0.17	0.05
THz abs. (cm^{-1})	2.5	1	1	<0.1
transp. range (μm)	0.65-18	0.9-15	0.75-12	0.5-9
band gap (eV)	2.1	1.424	2.34	2.45
nonlin. coeff. (pm/V)	d_{22}=24.3	d_{14}=46.1	d_{36}=39.4	d_{36}=85
nonlin. ref. index n_2 $\frac{10^{-15}cm^2/W}{\text{at } \lambda\ (\mu m)}$	45 at 1.06	150 at 2.1	40 at 2.1	? at 2.1
FOM_1, long pulses	0.13	0.83	0.68	
FOM_2, ultrashort pl.	0.13	0.64	0.55	
FOM_3, Kerr-limited	0.004	0.014	0.047	

Table 11.2: Linear and nonlinear properties, and figures of merit (normalized to LiNbO3) of crystals transparent in the 0-4 THz range and most widely used for optical THz generation according to ref. [10]

Three Wave Interaction

$$\frac{d\hat{E}(\omega_1)}{dz} = -j\kappa_1 \hat{E}(\omega_3)\,\hat{E}^*(\omega_2)\,e^{-j\Delta kz},$$
$$\frac{d\hat{E}(\omega_2)}{dz} = -j\kappa_2 \hat{E}(\omega_3)\,\hat{E}^*(\omega_1)\,e^{-j\Delta kz},$$
$$\frac{d\hat{E}(\omega_3)}{dz} = -j\kappa_3 \hat{E}(\omega_1)\,\hat{E}(\omega_2)\,e^{+j\Delta kz},$$

$$\kappa_i = \omega_i d_{eff}/n_i c_0, \qquad \text{and} \qquad \Delta k = k_3 - k_1 - k_2.$$

Difference Frequency Generation

$$\omega_3 = \omega_0 + \Omega \text{ and } \omega_2 = \omega_0,$$

$$\Omega \text{ is a THz frequency}$$

Phase Mismatch (for collinear interaction)

$$\Delta k = \left.\frac{\partial k_{opt}(\omega)}{\partial \omega}\right|_{\omega_0} \Omega - k_{THz}(\Omega) = \left(\frac{1}{v_{g,opt}} - \frac{1}{v_{p,THz}}\right)\Omega$$

$$= \frac{\Omega}{c}\left(n_{g,opt} - n_{p,THz}\right).$$

For Lithium Niobate **2** **5**

→ **Broadband non collinear phase matching by tilted pulse fronts**

→ **Quasi-phase matching**

11.2.1 Optical rectification with tilted-pulse-fronts

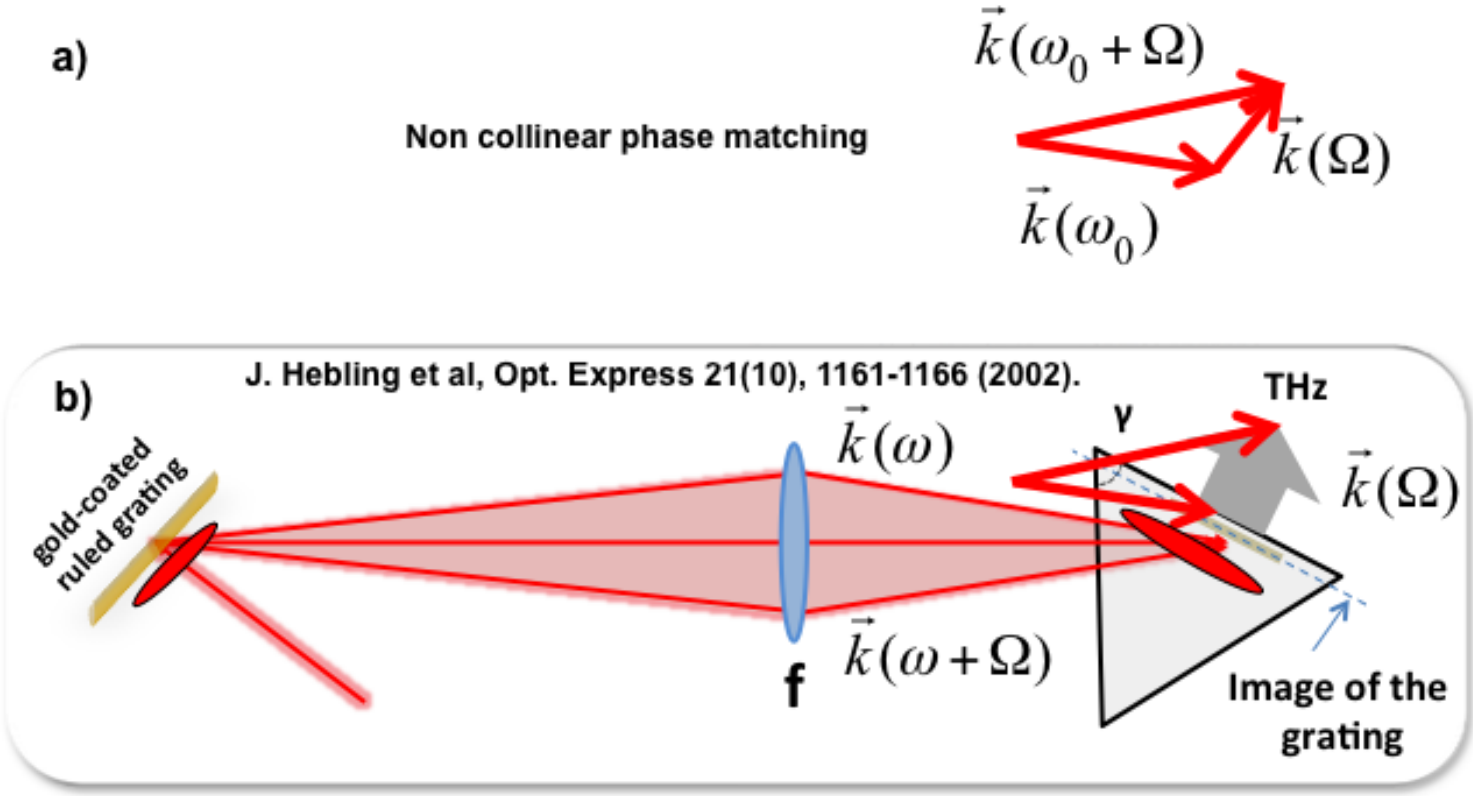

Figure 11.4: (a) Noncollinear phase matching for THz generation. Note, the THz phase index in lithium niobate is more than twice as large as the optical group index. (b) Broadband implementation of the noncollinear phase matching using a grating and imaging system that leads to the generation of pulses with a tilted pulse front.

Tilted pulse front technique

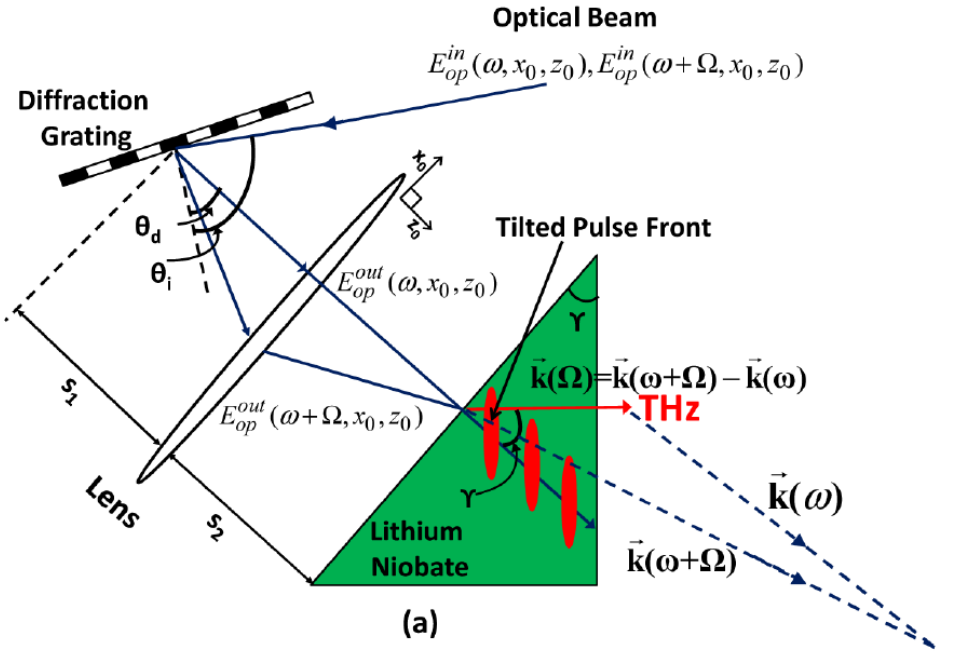

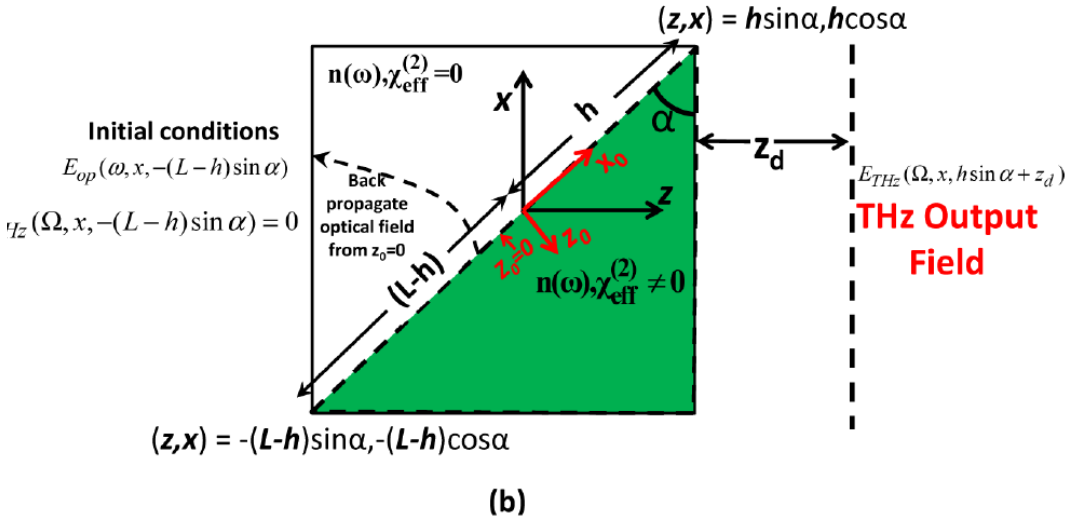

Non-collinear phase matching

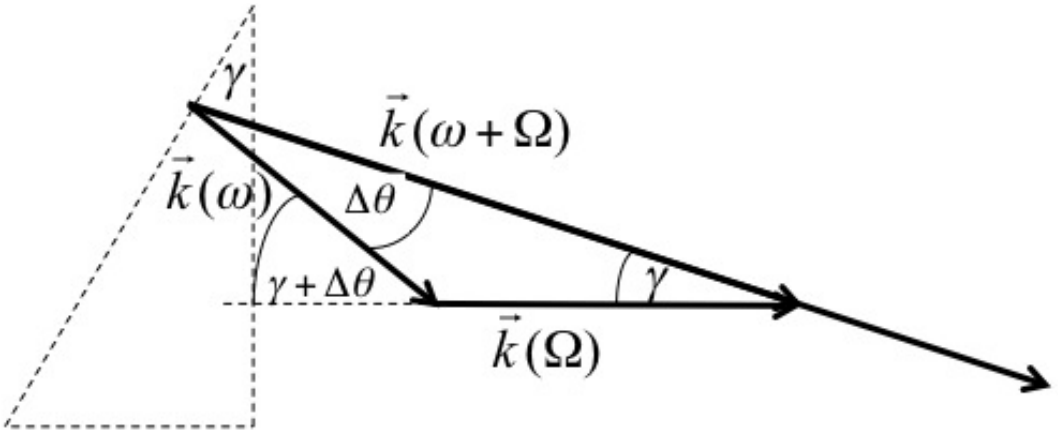

Figure 11.6: Noncollinear phase-matching condition for pulse-front-tilted optical rectification.

z - component

$$\begin{aligned}\Delta k_z(\omega) &= \cos\gamma\ k(\omega+\Omega) - \cos(\gamma+\theta(\omega))\ k(\omega) - k_{THz}(\Omega) \\ &= \cos\gamma\ \frac{\partial k_{opt}(\omega)}{\partial\omega}\Omega + \sin\gamma\left(-\frac{\partial\theta}{\partial\omega}\right)\Omega\ k(\omega) - k_{THz}(\Omega) = 0,\end{aligned}$$

y - component

$$\begin{aligned}\Delta k_y(\omega) &= \sin\gamma\ k(\omega+\Omega) - \sin(\gamma+\theta(\omega))\ k(\omega) \\ &= \sin\gamma\frac{\partial k_{opt}(\omega)}{\partial\omega}\Omega - \cos\gamma\frac{\partial\theta}{\partial\omega}\Omega\ k(\omega) \\ &= \sin\gamma\frac{\partial k_{opt}(\omega)}{\partial\omega}\Omega - \cos\gamma\left(-\frac{\partial\theta}{\partial\omega}\right)\Omega\ k(\omega) = 0.\end{aligned}$$

Tilt angle

$$\begin{aligned} \frac{\partial k_{opt}(\omega)}{\partial \omega}\Omega - \cos\gamma k_{THz}(\Omega) &= 0 \\ \frac{1}{v_{g,opt}} - \frac{1}{v_{p,THz}}\cos\gamma &= 0 \\ n_{g,opt} &= n_{p,THz}\ \cos\gamma, \end{aligned}$$

Necessary angular spread

$$\frac{\partial\theta}{\partial\omega} = -\tan\gamma\frac{v_{p,opt}}{\omega\ v_{g,opt}} = -\tan\gamma\frac{n_{g,opt}}{\omega\ n_{p,opt}}.$$

1D – spatial Model

$$\begin{aligned} k(\omega) &= \frac{1}{\cos\gamma}\frac{\omega\ n(\omega)}{c} + \frac{(\omega-\omega_0)^2}{2}k''_{AD} \\ k''_{AD} &= \frac{-n^2_{g,opt}(\omega_0)}{\omega_0\ c\ (\omega_0)}\tan^2\gamma. \end{aligned}$$

1D - Model

$$\frac{d\hat{E}_{THz}(\Omega,z)}{dz} = -\frac{\alpha_{THz}(\Omega)}{2}\hat{E}_{THz}(\Omega,z) - j\frac{\Omega\ d_{eff}}{c\ n_{p,THz}}\int_0^\infty \hat{E}_{opt}(\omega+\Omega,z)\ \ \hat{E}_{opt}(\omega,z)^*\ e^{j\Delta k(\omega)z}d\omega\ . \tag{11.13}$$

which also includes the THz absorption. For the optical field, we obtain

$$\begin{aligned}\frac{d\hat{E}_{opt}(\omega,z)}{dz} = & -\frac{\alpha_{opt}(\Omega)}{2}\hat{E}_{opt}(\omega,z) \\ & -j\frac{\omega\ d_{eff}}{c\ n_{p,opt}}\int_0^\infty \hat{E}_{opt}(\omega+\Omega,z)\ \ \hat{E}_{THz}(\Omega,z)^*\ d\Omega e^{-j\Delta k(\omega)z} \\ & -j\frac{\omega\ d_{eff}}{c\ n_{p,opt}}\int_0^\infty \hat{E}_{opt}(\omega-\Omega,z)\ \ \hat{E}_{THz}(\Omega,z)\ \ e^{-j\Delta k(\omega)z}d\Omega \\ & +\mathcal{F}\left[j\frac{\varepsilon_0\omega_0\ n_{p,opt}^2\ n_2 d_{eff}}{2}\left|E_{opt}(t,z)\right|^2\ \ E_{opt}(t,z)\right] \\ & +\mathcal{F}\left[j\frac{\varepsilon_0\omega_0\ n_{p,opt}^2\ n_2 d_{eff}}{2}\left[\left|E_{opt}(t-t',z)\right|^2\otimes h_r(t')\right]\ \ E_{opt}(t,z)\right],\end{aligned} \tag{11.14}$$

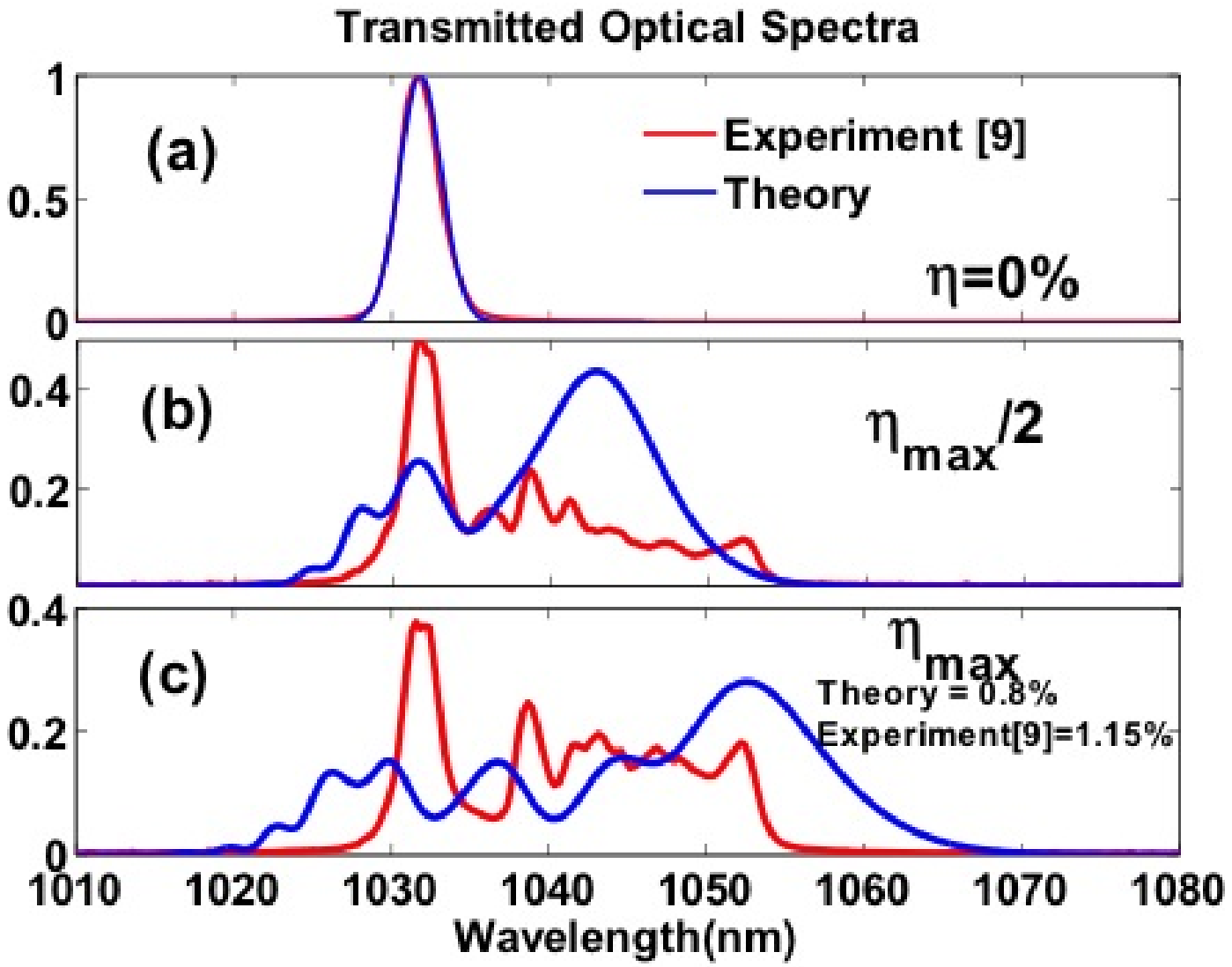

Figure 11.7: Comparison of experimental and simulated optical spectra for different amounts of generated THz.

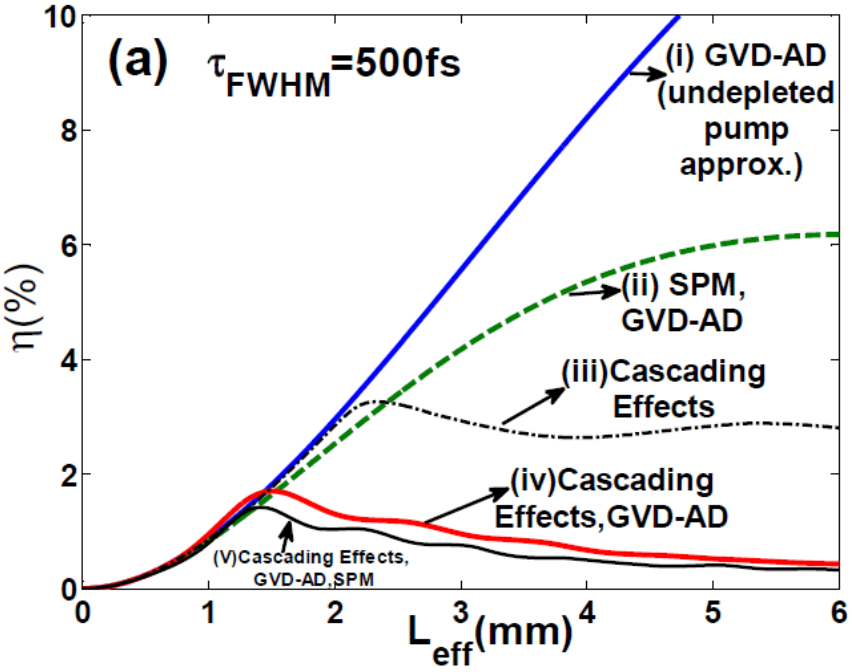

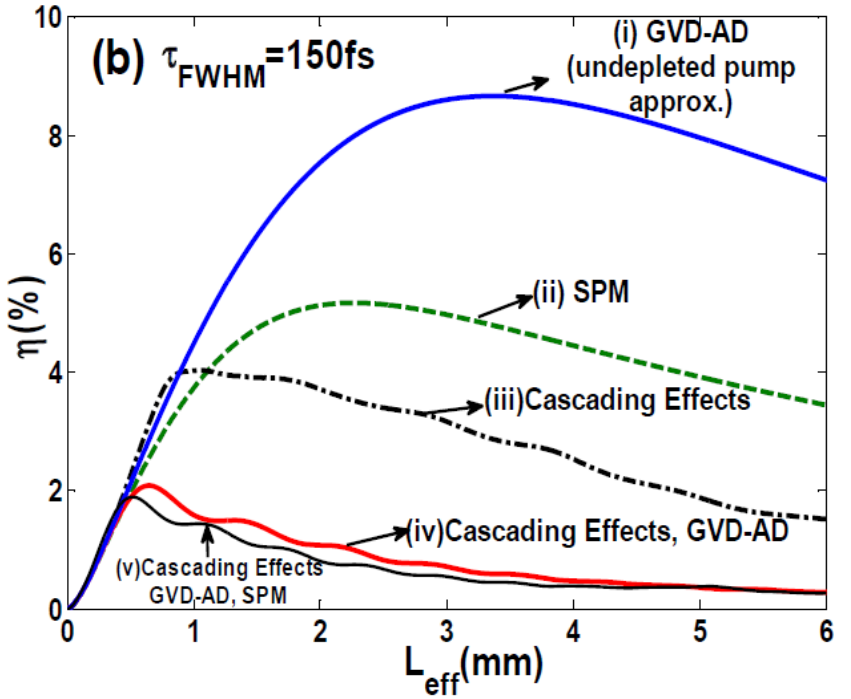

Figure 11.8: Conversion efficiencies as a function of effective length are calculated by switching on/off various effects. Material dispersion and absorption are considered for all cases. The pump fluence is 20 mJ/cm2, for a crystal temperature of 100 K. (a) Gaussian pulses with 500-fs FWHM pulse width with peak intensity of 40 GW/cm2 are used. Cascading effects together with GVD-AD leads to the lowest conversion efficiencies. The drop in conversion efficiency is attributed to the enhancement of phase mismatch caused by dispersion due to the large spectral broadening caused by THz generation (See Figs. 11.7(b)-(c)). However, since group velocity dispersion due to angular dispersion (GVD-AD) is more significant than GVD due to material dispersion at optical frequencies in lithium niobate, cascading effects in conjunc- tion with GVD-AD is the strongest limitation to THz generation. SPM effects are much less detrimental since they cause relatively small broadening of the optical pump spectrum (see 11.7 (a)). (b) Cascading effects along with GVD-AD are most detrimental even for a 150-fs Gaussian pulse with 3× larger peak intensity. [19]

2D - Simulation

(a) SPM, GVD-AD, material dispersion, absorption

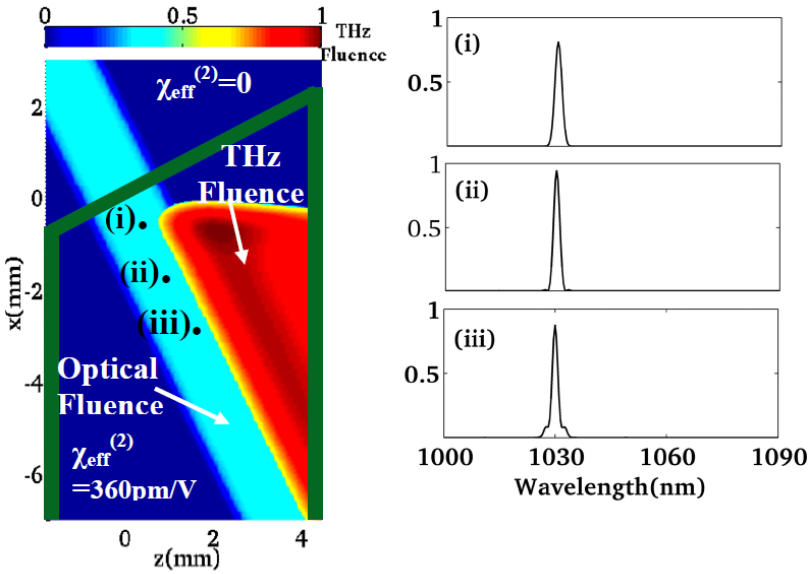

(b) Cascading Effects, GVD-AD, material dispersion, absorption

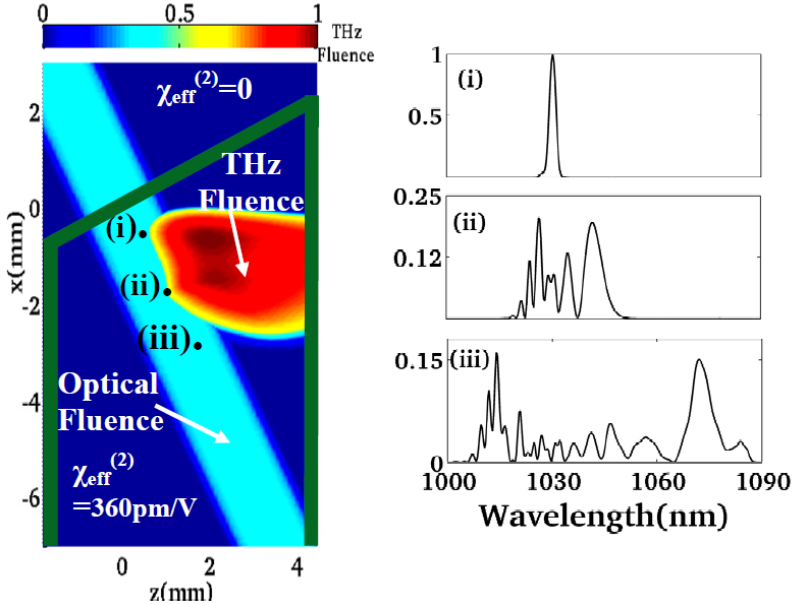

11.2.2 Optical rectification by Quasi-Phase Matching (QPM)

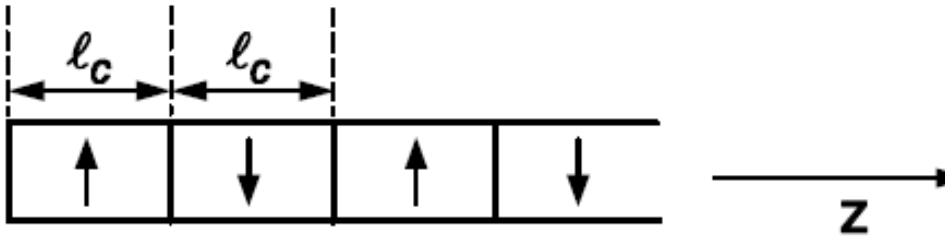

Periodically poled crystal

$$d_{eff}(z) = \sum_{m=-\infty}^{+\infty} d_m e^{jm\kappa z}$$

$$\begin{aligned}
\Delta k &= \left.\frac{\partial k_{opt}(\omega)}{\partial \omega}\right|_{\omega_0} \Omega - k_{THz}(\Omega) + m\frac{2\pi}{\Lambda} = \left(\frac{1}{v_{g,opt}} - \frac{1}{v_{p,THz}}\right)\Omega + m\frac{2\pi}{\Lambda} \\
&= \left(\frac{n_{g,opt} - n_{p,THz}}{c}\right)\Omega + m\frac{2\pi}{\Lambda} = 0 \\
\rightarrow \quad & \Lambda = m\frac{\lambda_{THz}}{n_{p,THz} - n_{g,opt}}.
\end{aligned}$$

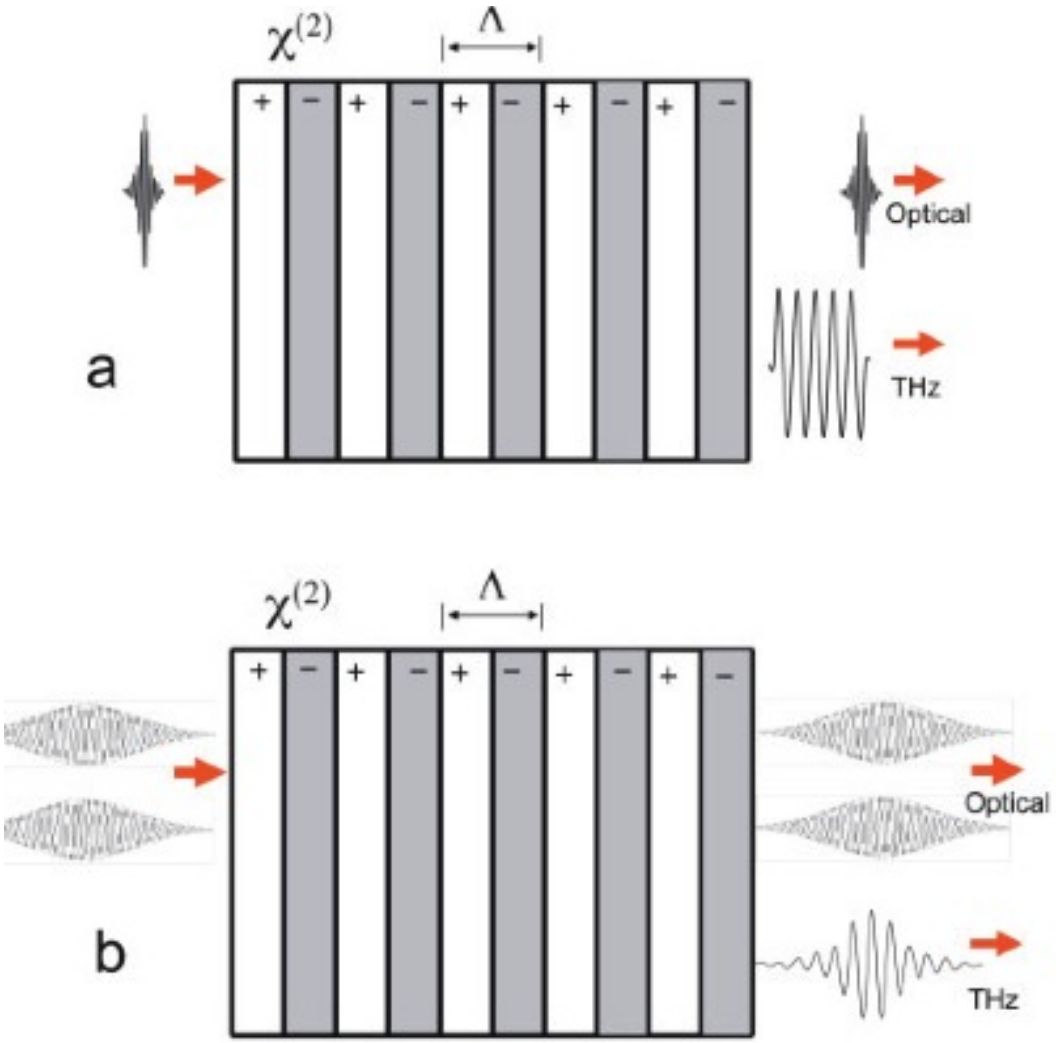

Figure 11.10: Schematic illustration of collinear THz-wave generation in a nonlin- ear crystal with periodically inverted sign of χ(2). (a) Optical rectification with femtosecond pulses, (b) difference-frequency generation with two picosecond pulses (Ω = ω3 − ω2) [10].

Plane-wave analysis of optical-to-THz conversion in QPM crystals with ultrashort pulses

$$E_{opt}(t) = Re\{E_0\ e^{-t^2/\tau^2}\ e^{j\omega_0 t}\} = \frac{1}{2}\{E_0\ e^{-t^2/\tau^2}\ e^{j\omega_0 t} + c.c.\},$$

$$\hat{E}_{opt}(\omega) = \frac{E_o \tau}{2\sqrt{\pi}} \exp\left(-\frac{\tau^2\omega^2}{4}\right)$$

$$\begin{aligned}\frac{d\hat{E}_{THz}(\Omega, z)}{dz} &= -j\frac{\Omega\ d_{eff}^{QPM}}{c\ n_{p,THz}}\frac{E_o^2\tau^2}{4\pi}\int_{-\infty}^{+\infty}\exp\left(-\frac{\tau^2(\omega+\Omega)^2}{4}\right)\exp\left(-\frac{\tau^2\omega^2}{4}\right)d\omega \\ &= -j\frac{\Omega\ d_{eff}^{QPM}}{c\ n_{p,THz}}\frac{E_o^2\tau}{2\sqrt{2\pi}}\exp\left(-\frac{\tau^2\Omega^2}{8}\right)\ e^{j\Delta k(\Omega)z}. \qquad (11.23)\end{aligned}$$

$$\left|\hat{E}_{THz}(\Omega, z)\right|^2 = \frac{\Omega^2\ d_{eff}^{QPM,2}}{c^2\ n_{p,THz}^2}\frac{E_o^4\tau^2}{8\pi}\exp\left(-\frac{\tau^2\Omega^2}{4}\right)\ L^2\mathrm{sinc}^2\left(\frac{\Delta k(\Omega)L}{2}\right) \qquad (11.24)$$

$$\text{with } \Delta k(\Omega) = \Delta k = \frac{n_{g,opt} - n_{p,THz}}{c} + m\frac{2\pi}{\Lambda} \qquad (11.25)$$

$$d_{eff}^{QPM} = \frac{2}{\pi}d_{eff}$$